BASIC SCIENCES



Trimethylamine-N-Oxide Affects Cell Type-Specific Pathways and Networks in Mouse Aorta to Promote Atherosclerotic Plaque Vulnerability

BACKGROUND: Trimethylamine-*N*-oxide (TMAO) has been significantly linked to atherosclerosis via several mechanisms, but its direct effect on the atherosclerosis-prone vasculature remains unclear. The objective of this study was to characterize the cell type-dependent and independent effects of TMAO on key vascular cell types involved in atherosclerosis progression in vivo.

METHODS: We performed single-cell RNA-sequencing on aortic athero-prone regions of female *Ldlr* mice fed normal laboratory, high-cholesterol, or high-cholesterol+TMAO diets for 3 months to identify which aortic cell types, differentially expressed genes, and biological pathways are affected by TMAO. We also modeled cell-cell communications and intracellular gene regulatory networks to identify gene networks perturbed by TMAO feeding. Key genes and pathways were validated using human vascular smooth muscle cells (vSMCs) exposed to TMAO. Changes in fibrous cap thickness, macrophage content, and collagen deposition in response to TMAO were measured with immunostaining and histology and quantified.

RESULTS: Our single-cell RNA-sequencing analysis revealed that TMAO supplementation upregulated apoptotic gene signatures and downregulated extracellular matrix (ECM) organization and collagen formation genes in a subset of atherosclerosis-specific modulated vSMCs. We also identified degradation of the ECM as a top pathway for vSMC-derived macrophage differentially expressed genes in response to TMAO. Network analyses supported that macrophage-vSMC communication mediates ECM remodeling. Using human smooth muscle cells exposed to TMAO in vitro, we confirmed the direct effect of TMAO on regulating collagen and apoptotic genes. In agreement with the changes in these pathways that affect plaque stability, we observed a significant decrease in fibrous cap thickness and collagen deposition in mice supplemented with TMAO.

CONCLUSIONS: Our results reveal the effects of TMAO on vSMCs to promote apoptosis and decrease ECM formation and on macrophage-mediated ECM degradation to, in concert enhance atherosclerotic plaque instability.

GRAPHIC ABSTRACT: A graphic abstract is available for this article.

Key Words: aorta ■ atherosclerosis ■ gene regulatory networks ■ mice ■ plaque, atherosclerotic ■ single-cell RNA-sequencing ■ TMAO

he diet is a major environmental exposure that influences metabolism and shapes gut microbial composition. The gut microbiome, in turn, participates in nutrient metabolism, leading to the generation of biologically active metabolites to modulate host physiology

and health.¹ Certain gut microbiota-derived metabolites have been increasingly recognized as either protective or risk factors in the development and progression of various cardiometabolic diseases. One such microbial metabolite is trimethylamine-*N*-oxide (TMAO), which has

Correspondence to: Xia Yang, PhD, Department of Integrative Biology and Physiology, University of California, 610 Charles E Young Dr E, Los Angeles, CA 90095. Email xyang123@ucla.edu

*D.M. Shih and X. Yang contributed equally.

Supplemental Material is available at https://www.ahajournals.org/doi/suppl/10.1161/ATVBAHA.125.323047. For Sources of Funding and Disclosures, see page 1797.

© 2025 The Authors. Arteriosclerosis, Thrombosis, and Vascular Biology is published on behalf of the American Heart Association, Inc., by Wolters Kluwer Health, Inc. This is an open access article under the terms of the Creative Commons Attribution Non-Commercial-NoDerivs License, which permits use, distribution, and reproduction in any medium, provided that the original work is properly cited, the use is noncommercial, and no modifications or adaptations are made.

Arterioscler Thromb Vasc Biol is available at www.ahajournals.org/journal/atvb

Nonstandard Abbreviations and Acronyms

DAPI 4',6-diamidino-2-phenylindole **DEG** differentially expressed gene

ECM extracellular matrix

FMO3 flavin monooxygenase 3

GRN gene regulatory network

HC high-cholesterol

MMP matrix metalloproteinase

NFκB nuclear factor-κB
NL normal laboratory

NLRP3 NLR family pyrin domain—containing 3

scRNAseqsingle-cell RNA-sequencingTGFtransforming growth factorTMAOtrimethylamine-N-oxidevSMCvascular smooth muscle cell

been significantly associated with or shown to be causal for numerous cardiovascular diseases and outcomes, including atherosclerosis, abdominal aortic aneurysm, thrombosis risk, incident major adverse cardiovascular events, and heart failure.^{2–7} Trimethylamine lyase metabolizes dietary choline, phosphatidylcholine, and L-carnitine, which are abundant in red meat and full-fat dairy products, to produce trimethylamine. Trimethylamine is subsequently absorbed by the host and metabolized to TMAO by hepatic FMO3 (flavin monooxygenase 3).⁸

TMAO is an independent predictor of high atherosclerotic burden in human patients and has been demonstrated to increase atherosclerotic lesion size and foam cell formation in mice.^{2,9} Mechanistically, TMAO has been linked to atherosclerosis through several atherogenic pathways. First, TMAO alters host sterol and lipid metabolism by induction of scavenger receptors CD36 and SRA1 on macrophages.2 This results in increased foam cell formation as well as alterations in systemic cholesterol metabolism 10-12 Second, TMAO has been shown to exert a proinflammatory effect on vascular cells. Aortas of Ldlr-/- mice fed a high-choline diet exhibited elevated inflammatory gene expression. Also, primary human aortic endothelial cells and vascular smooth muscle cells (vSMCs) treated with TMAO exhibited activation of NFκB (nuclear factor-κB) signaling and leukocyte binding to endothelial cells. 13 In endothelial cells and ApoE-/- mouse aortas, TMAO activated the NLRP3 (NLR family pyrin domain-containing 3) inflammasome and stimulated the generation of mitochondrial reactive oxygen species. 14,15 In vSMCs, TMAO induced NOX4 expression and reactive oxygen species production to promote vascular inflammation.¹⁶ Third, in patients with coronary artery disease, plasma TMAO levels were positively correlated with rupture. 17 In the tandem stenosis mouse model of atherosclerotic plaque instability, plasma

Highlights

- Single-cell RNA-sequencing of the aortic atheroprone regions in female Ldlr/- mice supplemented with trimethylamine-N-oxide (TMAO) in the diet revealed the effect of TMAO across cell types, particularly in vascular smooth muscle cell-derived macrophages and atheroprotective modulated vascular smooth muscle cells.
- TMAO increased apoptotic gene signatures and reduced ECM (extracellular matrix) organization and collagen formation gene signatures in modulated vascular smooth muscle cells in vivo, and in vitro exposure studies supported a direct effect of TMAO on these genes.
- Intracellular gene regulatory networks and cell-cell communication predictions offered insights into the regulatory cascades within and across cell types impacted by TMAO.
- Fibrous cap thickness and collagen deposition, markers of atherosclerotic plaque stability, were significantly reduced in female Ldlr^{-/-} mice fed highcholesterol+TMAO versus high-cholesterol diets for 5 months.

TMAO levels correlated with plaque instability characteristics, including inflammation, platelet activation, and intraplaque hemorrhage, whereas a reduction in TMAO enhanced carotid plaque stability. TMAO also limited macrophage M2 polarization and efferocytosis in vitro.

The above mechanisms, involving modulation of cholesterol metabolism and inflammation, partially explain how TMAO exerts its proatherogenic and prorupture effects. We now report our single-cell RNA-sequencing (scRNAseq) study, which investigates the effects of TMAO on vascular cells in the context of atherosclerosis using low-density lipoprotein receptor-deficient (*Ldlr*/-) mice. Our results show that TMAO supplementation in the diet reduces the formation and increases the degradation of extracellular matrix in atherosclerotic lesions, thereby destabilizing lesions and making them more prone to rupture. In particular, we address these effects in a fibroblast-like vSMC subset, termed modulated vSMCs, that are transcriptionally distinct from contractile vSMCs.²⁰

METHODS

Data Availability

All data and materials have been made publicly available at the Gene Expression Omnibus repository and can be accessed with the series record GSE290376.

Animals and Dietary Treatment

All animal experiments were approved by the University of California, Los Angeles Animal Care and Use Committee.

Female Ldlr^{-/-} (B6.129S7-Ldlr^{tm1Her}/J; stock: 2207) mice were obtained from the Jackson Laboratory and maintained on a 12-hour light-dark cycle from 6 AM to 6 PM. Female mice were used in this study because they develop larger lesions compared with males and are typically used for atherosclerosis studies. 21,22 Mice were divided into 3 diet groups: (1) normal laboratory (NL) diet group (catalog no. TD.2018: 24% protein, 18% fat, 58% carbohydrate; Teklad Global 18% Protein Rodent Diet, Teklad, Madison, WI), 14 weeks of age; (2) 0.5% high-cholesterol (HC) diet group (catalog no. TD.170261: 994.7 g Teklad Global 18% Protein Rodent Diet/Kg diet, 5.0 g cholesterol/Kg diet; Teklad); (3) 0.5% cholesterol+0.125% TMAO diet (HC+TMAO diet: catalog no. TD.210189: 992.9 g Teklad Global 18% Protein Rodent Diet/kg diet, 1.8 g TMAO/ kg diet, 5.0 g cholesterol/Kg diet; Teklad). The 0.125% TMAO was similar in concentration to a previous study.2 Mice were fed the HC and HC+TMAO diets at 10 weeks of age for 12 weeks. We focus on the TMAO effect in the current study (HC+TMAO versus HC); HC versus NL comparison only served to confirm previous findings on cell types and pathways involved in atherosclerosis. Mouse euthanasia was performed by isoflurane overdose followed by cervical dislocation. On euthanasia, mice were perfused with PBS, and tissues were weighed and instantly frozen in liquid nitrogen. The ascending aorta, aortic arch, and thoracic aorta were isolated and prepared for scRNAseg.

Aorta Dissection and Single-Cell Dissociation

Each diet group consisted of 3 aorta pools with n=2 mice/ pool, for a total of 9 independent biological replicates from 18 mice (n=6 mice/group). The sample size is similar to previous mouse aorta scRNAseq studies. 20,23-25 Aorta samples from the above groups were collected from the lesion-prone areas of aorta, including the ascending aorta, aortic arch, and thoracic aorta. Aorta cell dissociation protocol was based on Wirka et al.20 Briefly, the aorta samples were cut into <1 mm pieces and incubated in 1 mL of Hanks' Balanced Salt solution containing 2 units of Liberase and 24 units of elastase at 37 °C for 1 hour. Fetal bovine serum (10% of total volume) was then added to inactivate the enzymes. The digested cells were then passed through a 70 µm cell strainer and rinsed with 4 mL PBS. After centrifugation at 300g, 4°C, for 10 min, the supernatant was discarded. The cells were then resuspended in 4 mL PBS/0.04% BSA (bovine serum albumin), spun down again, and resuspended in 100 µL PBS/0.04% BSA.

scRNAseq Library Construction and Sequencing

Approximately 16000 aortic cells pooled from 2 mice within the same diet group were used for each single-cell library construction. In total, 9 independent libraries representing 18 mice (3 libraries from 6 mice/diet group) were made using the 10x Genomics Chromium Next GEM Single-Cell 3' Kit v3.1. All samples were processed in 1 batch, and the 9 libraries were then sequenced in 1 lane of NovaSeq S4 2×100 bp at 2.4 billion reads.

scRNAseq Data Preprocessing and Quality Control

Fastq files from each mouse aorta pool were individually aligned to the *Mus musculus* genome assembly Genome

Reference Consortium Mouse Build 38 (GRCm38 mm10) using CellRanger version 6.0.1 (10X Genomics). CellBender was used to learn the background noise profile and differentiate cell-containing droplets from cell-free droplets.²⁶ A digital gene expression matrix, in which each row represents the read count of a gene and each column corresponds to a unique single cell, was generated from each library's filtered feature-barcode data sets and was subsequently analyzed using the R package Seurat version 4.3.0.27 Single cells were selected based on a threshold of between 200 and 5000 genes expressed and between 500 and 20000 unique molecular identifiers. Further filtering was performed with a mitochondrial gene expression cutoff of <15% and a hemoglobin gene expression cutoff of <0.1% to remove poor-quality or contaminated cells. Raw transcript counts of each gene were normalized relative to the total number of read counts in that cell, and the resulting values were multiplied by 10000 and log-transformed.

Cell Clustering and Cell Type Annotation and Distribution

Single cells were projected onto 2 dimensions for visualization using Uniform Manifold Approximation and Projection and assigned into clusters using Louvain clustering. 27,28 Nonparametric Wilcoxon rank-sum test was used to determine cluster-specific marker genes consistent across samples and expressed in at least 10% of the cells in each cluster of interest. To resolve the identities of the cell clusters, cluster-specific marker genes were evaluated for convergence on known aorta cell type marker genes curated from previous studies, including Wirka et al, Cochain et al, Kan et al, and Kim et al. 20,24,29,30 vSMCs and macrophages were further extracted to identify known subtypes within each cell type. Cell clustering patterns between samples within-group and between-group were examined to assess technical versus biological contributions. Cell type proportion analysis was performed with the Propeller package in R.31 Significant differences between HC versus NL and HC+TMAO versus HC in the same cell (sub)type were evaluated by unpaired t test, and false discovery rate was calculated with the Benjamini-Hochberg method.

Trajectory Analysis

Trajectory analysis of vSMCs and vSMC-derived macrophages was performed using the Slingshot package in R, which predicts pseudotime and cell lineages from scRNAseq data.³² vSMC 1, representing classic contractile vSMCs, was classified as the start cluster. Slingshot functions getLineages and getCurves were used to identify the global lineage structure with a minimum spanning tree and to fit curves describing the lineage, respectively.

Differential Gene Expression Analysis and Pathway Enrichment

Genes expressed in at least 10% of single cells for each individual cluster were considered for differential expression analysis. Nonparametric Wilcoxon rank-sum test was used to compare gene expression between dietary groups to identify differentially expressed genes (DEGs) in each cell cluster. We corrected for multiple testing with the Bonferroni method, and DEGs with at least a 0.1 log2-fold change in gene expression

between groups and with Bonferroni-adjusted P<0.05 were included in downstream pathway enrichment analysis utilizing pathways from Reactome.33,34 However, for clusters with an insufficient number of DEGs at false discovery rate <0.05 to identify meaningful significant pathways, DEGs with a threshold of P<0.01 were used to predict suggestive pathways for these cell types. Significant enrichment of pathways was based on a hypergeometric test followed by multiple testing correction with the Benjamini-Hochberg method. To confirm the cell-level DEG results, we also performed metacell-based DEG analysis, aggregating subsets of similarly expressing cells within each cell type and sample. The metacell approach has been shown to identify robust DEGs between conditions. 35,36 We used the metacell approach in high-dimensional weighted gene coexpression analysis, which calculates the k-nearest neighbors for each cell within a sample's cell type and averages their gene expression counts. $\!\!^{37}$ We used the standard parameters of high-dimensional weighted gene coexpression analysis, which enforces 25 cells per metacell, at most 10 cells shared between any 2 metacells, at least 100 cells within a cell type to perform metacell analysis, and at most 1000 metacells within a cell type for each sample. We derived 3895 metacells for the NL mice, 3088 metacells for the HC mice, and 3834 metacells for the HC+TMAO mice. To visualize the lowerdimensional representation of the metacells, we performed standard log normalization, scaling, principal component analysis, and Uniform Manifold Approximation and Projection. For differential gene expression analysis, we normalized the metacell counts and performed Wilcoxon rank-sum tests with Bonferroni multiple testing correction. We chose metacell over pseudobulking because it preserves biological heterogeneity within the cell type, which is removed in pseudobulking.35 However, we also performed pseudobulk DEG analyses using DESeq2.38

Single-Cell Gene Regulatory Network Construction

The single-cell network inference method (SCING) was used to construct cell type-specific intracellular global gene regulatory networks (GRN) from the scRNAseq raw counts matrix using gradient boosting.³⁹ SCING first pseudobulk cells into metacells through Leiden clustering to mitigate scRNAseq gene sparsity and constructs a consensus GRN across subsamples of the data via bootstrapping. We identified highly connected subnetworks, or modules, using Leiden clustering with the final GRN. Expression profiles of GRN modules were generated using the module eigengene approach from hdW-GCNA (high-dimensional weighted gene coexpression analysis).³⁷ Differential module eigengenes were calculated using the Wilcoxon rank-sum test with FindDMEs in hdWGCNA. Multiple testing was accounted for with the Bonferroni method. Cytoscape (v. 3.8.2) was used for network visualization.⁴⁰

Cell-Cell Communication Network Construction

CellChat was used to predict alterations in cell-cell communication in response to TMAO.⁴¹ CellChat objects were created for HC+TMAO and HC conditions separately using endothelial cells, fibroblasts, vSMC subsets, and macrophage subsets. The total number of interactions of the inferred cell-cell communication networks from HC+TMAO and HC conditions were then

compared. We also used CellChat to determine specific cell-cell signaling changes of modulated vSMCs between HC+TMAO and HC groups. To predict upstream ligands that may regulate the HC+TMAO versus HC DEGs, we used NicheNet, 42 where modulated vSMCs were set as the receiver cell type, and the HC+TMAO versus HC modulated vSMC DEGs were input as the targets. We focused on vSMC DEGs involved in ECM organization, collagen formation, and apoptosis due to their significance in pathway analysis. We also carried out NicheNet analysis on macrophages, where macrophage subtypes and the HC+TMAO versus HC DEGs for each macrophage subtype were set as the targets. The sender cell types included macrophage subtypes, vSMC subtypes, endothelial cells, and fibroblasts.

In vitro Validation of the Direct Effect of TMAO on Key vSMC and Macrophage Genes

Human immortalized coronary artery vSMCs (gift from Dr Clint Miller, University of Virginia, Charlottesville, VA) and human primary aortic vSMCs (PCS-100-012; ATCC) were cultured in vSMC growth medium with premixed supplements (catalog no. C-22062; PromoCell). RAW 264.7 mouse macrophage cells (ATCC, Manassas, VA) were cultured in DMEM medium supplemented with 5% FBS, 100 U/mL penicillin, and 100 µg/mL streptomycin. Cells were grown in 6-well plates overnight, followed by stimulus with various concentrations of TMAO (100, 200, or 400 µmol/L) or vehicle (PBS) in growth media for 24 hours before harvest. TMAO concentrations were selected to reflect normal physiologically relevant and elevated pathological conditions and were likewise used in our previously published work. 13 All cell culture experiments were performed in triplicate to confirm the robust direct function of TMAO. Cells were homogenized in TRIzol (Qiagen), and RNA extraction was performed according to the manufacturer's protocol. RNA samples were reverse transcribed using a high-capacity cDNA reverse transcription kit (Applied Biosystems, Waltham, MA). Quantitative polymerase chain reaction was performed using the PowerUp SYBR Green Master Mix (catalog no. A25778; Applied Biosystems) for select target genes from the scRNAseq analysis. All quantitative polymerase chain reaction primer sequences are listed in Table S1. Housekeeping genes included Rpl13a for RAW 264.7 mouse macrophage cells, B2M for human immortalized coronary artery vSMCs, and SRSF4 for human primary aortic vSMCs. The housekeeping genes were confirmed not to show differential expression in our scRNAseg data. Differences in the expression level of each gene between diet groups were determined by 1-way ANOVA.

Immunofluorescence Staining to Validate the Effect of TMAO on Fibrous Cap Thickness In Vivo

Female $LdIr^{-/-}$ female mice were fed HC+TMAO or HC diets for 5 months (n=6/group) to allow for the development of the fibrous cap. Aortic root was collected for fibrous cap measurements. OCT-embedded aortic root tissues were sectioned at a thickness of 10 μ m with 3 sections per slide. Slides were fixed in 4% paraformaldehyde at room temperature, permeabilized with Triton X-100 on ice, and blocked for 1 hour at room

temperature with a mixture of PBS, 3% BSA powder, and 5% goat serum. Slides were then incubated with Tagln (transgelin) primary antibody (1:200, ab14106; Abcam) and CD68 (cluster of differentiation 68) primary antibody (1:400, MCA1957GA; Biorad) to stain for fibrous cap or 10x-diluted block solution as negative control. Each slide had 2 sections stained with the primary antibody and 1 section used for negative control. Goatantirabbit 488 (1:500, A11008; Thermo Fisher Scientific) and goat-antirabbit 594 (1:500, A11012; Thermo Fisher Scientific) were used as secondary antibodies for immunofluorescence for transgelin and CD68, respectively. Slides were washed in PBS baths between antibody steps. Slides were mounted with DAPI (4',6-diamidino-2-phenylindole; Sigma Aldrich). All immunostainings were captured with Zeiss (Axioskop 2 plus, Carl Zeiss, Heidelberg, Germany) or Keyence BZ-X (Keyence, Itasca, IL) microscopes. Fibrous cap measurement was performed based on Newman et al.43 The fibrous cap area of measurement was determined by the presence of TagIn+ cells. Using ImageJ, we added 15 evenly spaced points along the lumen of female *Ldlr*^{-/-} mice fed HC+TMAO or HC diets. Lines covering the depth of the fibrous cap were drawn perpendicular to the points on the lumen, and the average of the lengths of the lines was calculated to determine the depth of the fibrous cap. CD68+ macrophage percentage was calculated as the ratio of costained red (CD68+) and blue (DAPI) cells over the total number of cells (DAPI). Differences between groups were determined by unpaired t test.

Masson's Trichrome Staining for Collagen Deposition Quantification

Masson's Trichrome staining was performed on frozen aortic root sections according to the manufacturer's protocol (catalog no. KTMTR; StatLab, TX). Frozen sections were equilibrated to room temperature for 20 minutes. Sections were then incubated with Bouin solution overnight at room temperature in a humidified chamber. The following day, slides were rinsed in running tap water for 3 minutes until the tissue became colorless. Sections were then stained with Working Weigert hematoxylin solution for 5 minutes, followed by a 2-minute rinse under running tap water. Next, sections were immersed in Biebrich scarlet-acid fuchsin solution for 15 minutes, rinsed in running tap water for 1 minute, and incubated in phosphomolybdic/phosphotungstic acid solution for 15 minutes. Without additional rinsing, slides were transferred directly into Aniline Blue solution for 10 minutes and rinsed in running tap water for 1 minute. Then, sections were immersed in 1% acetic acid for 5 minutes and mounted. Analysis of collagen deposition area in Masson's trichrome staining was performed in ImageJ. Differences between groups were determined by unpaired t

Statistics

The appropriate statistical tests were determined based on assessment of normality and homogeneity of variance. Comparisons of data following normal distribution between groups were performed by unpaired t test or ANOVA followed by Tukey post hoc test. Data that did not follow normal distribution were analyzed using the Wilcoxon rank-sum test. Multiple testing was corrected by the Bonferroni or Benjamini-Hochberg methods.

RESULTS

scRNAseq Identification of Distinct Cell Types in the LdIr^{-/-} Mouse Aorta

Female Ldlr-/- mice (n=6/group, 22 weeks of age at euthanasia) were fed HC or HC+TMAO diets for 3 months, and ascending aorta, aortic arch, and thoracic aorta were collected for scRNAseq; the same aortic tissues from control female *Ldlr*^{-/-} mice (14 weeks of age) were also collected for sequencing (Figure 1A). Plasma TMAO levels were significantly increased in mice fed the HC+TMAO diet compared with HC or NL diets (Figure 1B). We detected 10 main cell clusters that each displayed distinct gene expression patterns and represented major cell types within the lesion-prone areas of the aorta (Figure 1C through 1E). Known aortic cell types recovered included vSMCs, fibroblasts, macrophages, and endothelial cells. We also recovered small populations of pericytes, T cells, B cells, and neurons. Biological replicates within groups showed less variability in comparison to variability between groups, suggesting that main transcriptome differences were driven by biological variability between diet groups (Figure S1).

Subclustering of vSMCs identified 4 subtypes. These include 2 distinct classic contractile vSMC clusters, with vSMC1 expressing higher classic contractile vSMC markers (Acta2, Tagln, Myh11, Tpm1) and vSMC2 expressing higher levels of Atf3, Nr4a1, Gadd45g, and Gadd45b (Figure 1F and 1G). We further identified a distinct vSMC cluster highly expressing Rgs5, which may represent nonproliferative vSMCs that do not contribute to the fibrous cap (Figure 1G). Finally, we identified modulated vSMCs primarily present in HC+TMAO and HC samples and characterized by higher expression of Spp1, Fn1, Col2a1, Lum, and Lgals3 compared with other vSMC subtypes (Figure 1F and 1G). Consistent with previous findings, a small proportion of modulated vSMCs were present in the NL condition. Other than a nonsignificant trend towards decreased modulated vSMCs with TMAO feeding, the single-cell distribution from HC+TMAO versus HC mice was similar (Figure 1H; Table S2). As expected, modulated vSMCs and macrophages were significantly increased with the HC diet compared with NL, which parallels the presence of lesions (Figure 1H; Table S2).

We also subclustered the macrophage cell type, revealing monocytes and resident inflammatory, foamy *Trem2*+, and vSMC-derived macrophages (Figure 2A through 2D). vSMC-derived macrophages composed 29.1% of the TMAO-fed macrophage population, as compared with 27.7% in NL and 32% in HC groups (Figure 2E; Table S3). Proportions of foamy *Trem2*+ macrophages and monocytes were significantly increased in HC compared with NL (Figure 2E; Table S3). Trajectory analysis predicted vSMC-derived macrophages to derive from modulated vSMCs (Figure S2).

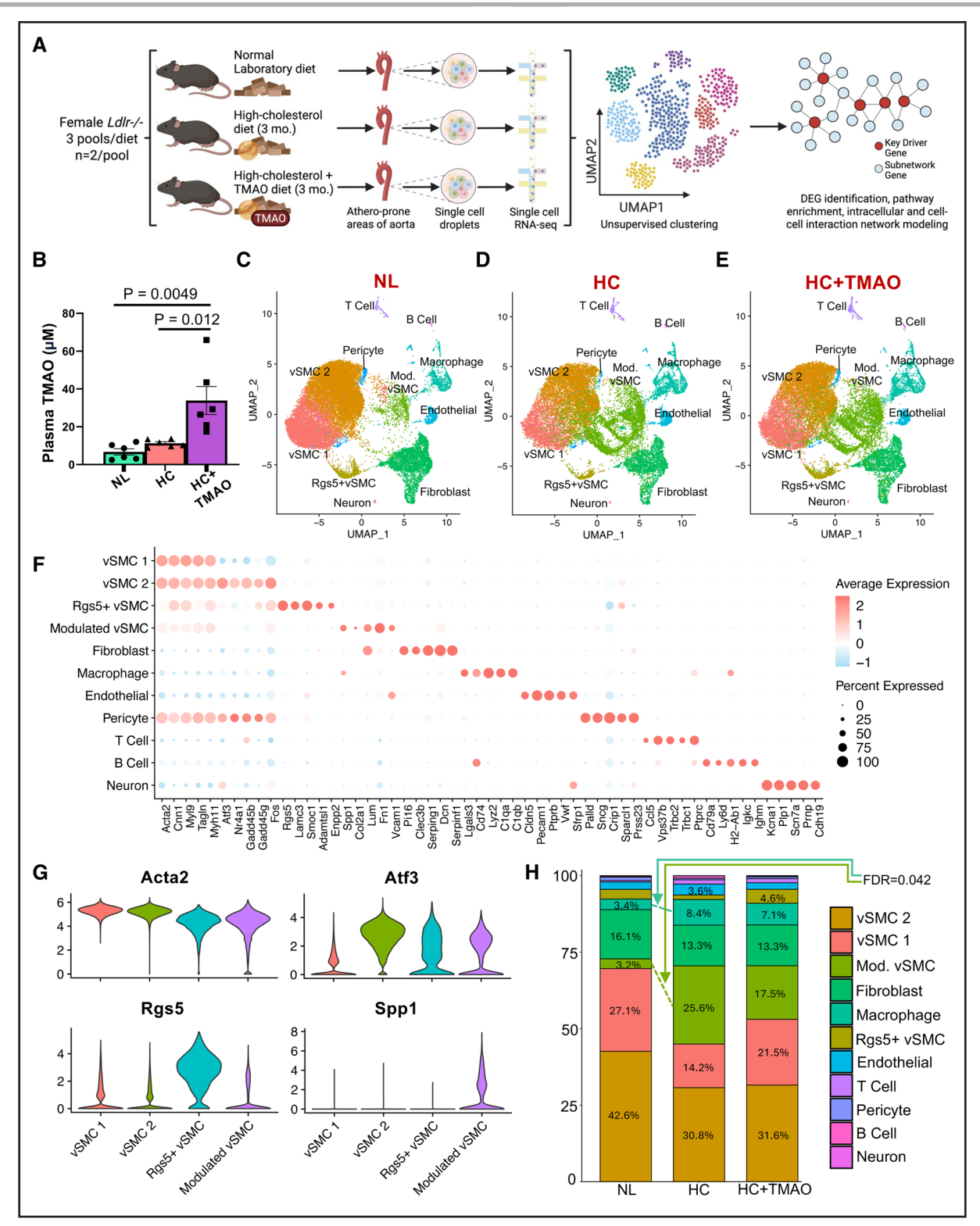


Figure 1. Identification of major aortic cell types and cell type-specific gene markers.

A, Schematic diagram of the study design. Athero-prone areas of the aorta (ascending aorta, aortic arch, and thoracic aorta) were collected from female Ldlr' mice on normal laboratory (NL), high-cholesterol (HC), or HC+ trimethylamine-*N*-oxide (TMAO) diets (n=6/group), and 2 mouse samples from the same diet group were pooled together, with n=3 pools/group. B, Plasma TMAO levels (µM) in the NL-, HC-, and HC+TMAO-fed mice as measured by mass spectrometry (n=6/group). Statistical significance was determined by unpaired *t* test. C through E, Uniform Manifold Approximation and Projection (UMAP) representation of cell clusters in NL, HC, and HC+TMAO conditions, respectively. F, Cluster-specific expression of previously known cell type markers. G, Normalized expression values of top markers of vascular smooth muscle cells (vSMC) subtype clusters: vSMC 1: *Acta2*, vSMC 2: *Atf3*, *Rgs5*⁺ vSMC: *Rgs5*, modulated vSMC: *Spp1*. H, Proportions of identified cell types within total cells recovered for each diet condition in order of abundance. Statistical significance was determined by unpaired *t* test. False discovery rate (FDR) was calculated with Benjamini-Hochberg. DEG indicates differentially expressed genes; and Mod. vSMC, modulated vSMC.

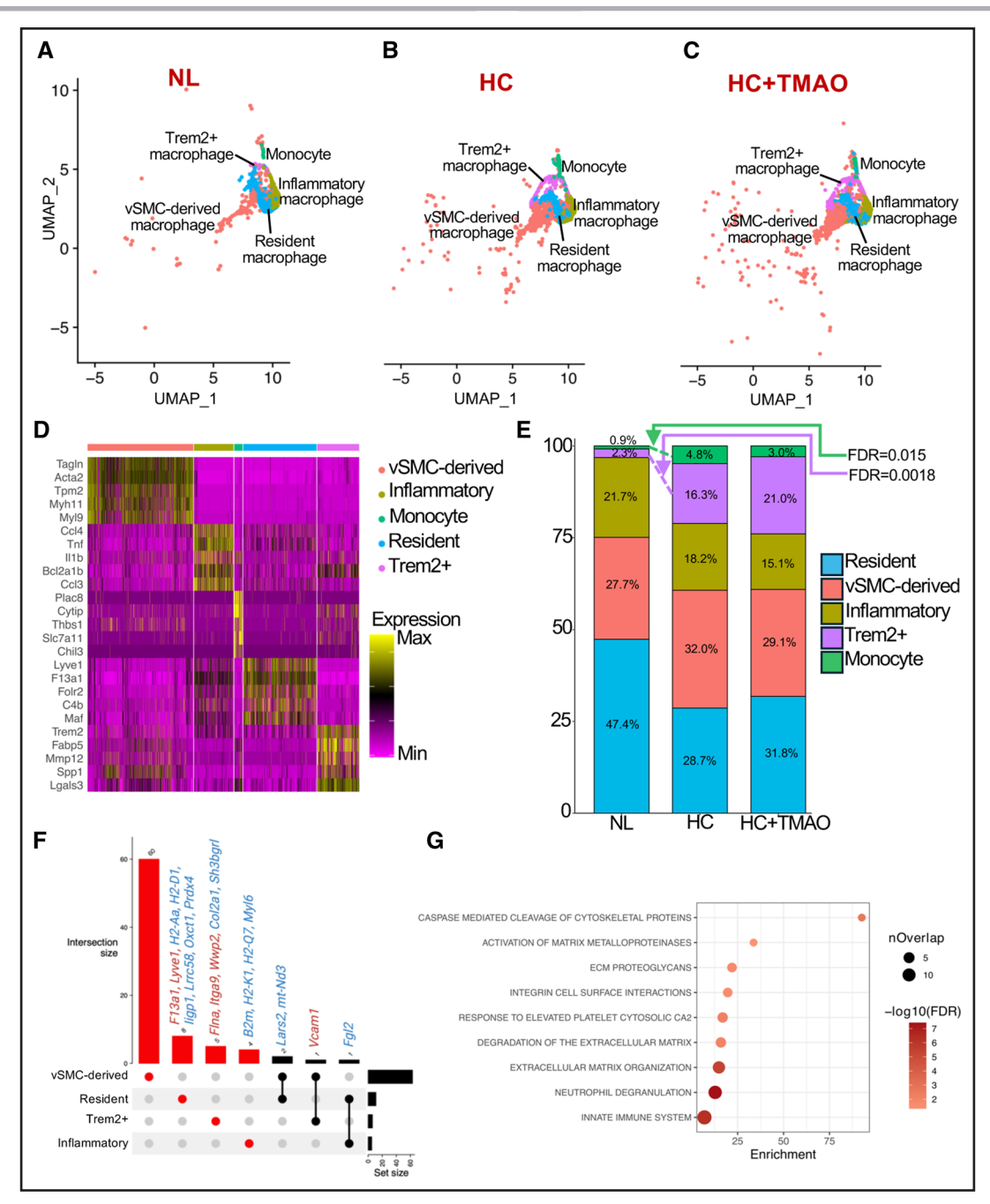


Figure 2. Identification of macrophage subtypes and differences in vascular smooth muscle cells (vSMC)-derived macrophages with trimethylamine-N-oxide (TMAO).

A through **C**, Uniform Manifold Approximation and Projection (UMAP) of macrophage subclusters in normal laboratory (NL), high-cholesterol (HC), and HC+TMAO conditions, respectively. **D**, Subcluster-specific expression of previously known macrophage subtype markers. **E**, Proportions of macrophage subtypes within total macrophage number recovered for each diet condition in order of abundance. Statistical significance was determined by unpaired *t* test. false discovery rate (FDR) was calculated with Benjamini-Hochberg. **F**, Shared and cell type-specific differentially expressed genes (DEGs; FDR<0.05) induced by TMAO feeding in macrophage subtypes. DEGs unique to a cell type are highlighted in red in the upset plot and histogram, and shared DEGs are indicated in black. The histogram above each plot indicates the DEG counts for each category. DEG direction is indicated by the color of the gene name: red: upregulated, blue: downregulated. **G**, Top representative pathways from Reactome enriched for vSMC-derived macrophage DEGs (FDR<0.05). ECM indicates extracellular matrix; Max, maximum expression; Min, minimum expression; and Trem2+, foamy *Trem2*+ macrophages.

Overall, our scRNAseq analysis revealed all expected aortic cell types and subtypes, as well as the increases in disease-associated vSMCs and macrophages in

atherosclerotic conditions. Importantly, compared with HC only, TMAO+HC exhibited trends towards decreased proportions of modulated vSMCs.

Confirmation of Key Atherogenic Genes and Pathways Between HC and NL Groups

We first identified DEGs between HC and NL groups, confirming the atherogenic effects of HC in our scRNA-seq data (Figure S3A; Table S4). For example, upregulated DEGs in modulated vSMCs were significantly enriched for ECM organization, programmed cell death, and platelet activation and aggregation (Figure S3B; Table S5). In modulated vSMCs, downregulated DEGs were significantly enriched for muscle contraction, supporting that vSMCs phenotypically switch from classic contractile towards a synthetic phenotype with atherosclerosis progression (Figure S3C; Table S6).

TMAO Impacts Shared and Cell Type-Specific Genes and Biological Pathways

To understand the ubiquitous and cell type-specific impact of elevated TMAO in lesions, we identified shared and cell type-specific DEGs between HC+TMAO and HC (Table S7). Across cell types, various mitochondriaencoded genes (eg, mt-Nd3, mt-Atp8, and mt-Nd2) were downregulated with the addition of TMAO, suggesting potential mitochondrial dysfunction and increased oxidative stress across cell types with TMAO (Figure 3A). Mitochondrial dysfunction can trigger various cellular stress responses, including apoptosis. In support of a direct effect of TMAO, human coronary artery vSMCs treated with varying concentrations of TMAO exhibited downregulation of ATP8 and ND3 (Figure 3D). Because TMAO supplementation in the diet can affect TMAOtrimethylamine conversion via Fmo2 (TMAO to trimethylamine) and Fmo3 (trimethylamine to TMAO), we found Fmo2 to be upregulated in 6 cell types and Fmo3 to be upregulated in 3 vSMC subtypes.

Among all cell types, modulated vSMCs exhibited the greatest number of DEGs (n=962) that are affected by TMAO, and the majority of DEGs were specific (n=722) to this atherosclerosis-associated vSMC subtype (Figure 3A). Upregulated modulated vSMC DEGs were enriched for respiratory electron transport (nuclear-encoded cyclooxygenase NADH: ubiquinone gene families), apoptosis, and P53related pathways (Figure 3B; Table S8). Trp53inp1, a proapoptotic P53 target gene, was upregulated in modulated vSMCs in vivo, and we confirmed a direct effect of TMAO on this gene in primary human vSMCs (Figure 3E). Previous work has shown that adenoviralmediated expression of p53 in mouse atherosclerotic lesions resulted in vSMC apoptosis, cap thinning, and increased vulnerability to rupture.44 Downregulated modulated vSMC DEGs were enriched for collagen biosynthesis and formation, ECM (extracellular matrix) organization, and signaling by receptor tyrosine kinases (Figure 3C; Table S9). We further confirmed the direct effect of TMAO on downregulating key collagen genes *COL1A1* and *COL1A2*, as well as regulator *TGFB1* (transforming growth factor beta 1) in primary human aortic vSMCs (Figure 3E). As phenotypically switched vSMCs contribute to lesion composition and largely compose the fibrous cap, reduced collagen and dysregulated ECM organization by TMAO may result in a more vulnerable fibrous cap. These results suggest that TMAO decreases collagen and ECM content and promotes apoptosis of phenotypically switched vSMCs, events that exacerbate lesion cap instability.

To confirm our cell-level DEG analysis results, we also applied a metacell approach, which aggregates subsets of similarly expressing cells to mitigate sparsity and technical variability while preserving the biological variability within a cell type³⁵⁻³⁷ (Figure S4A through S4C). We still observed the greatest number of DEGs in modulated vSMCs (Figure S4D; Table S10). Further, metacell-derived modulated vSMC DEGs were enriched for similar pathways as the cell-level DEGs (Figure S4E and S4F). We also performed pseudobulk DEG analyses, which yielded limited results (Table S11).

Macrophage subtypes also exhibited cell typespecific transcriptomic changes induced by TMAO feeding (Figure 2F; Table S12). Specifically, vSMCderived macrophage DEGs were significantly enriched for ECM- and immune-related pathways, activation of MMPs (matrix metalloproteinases), and caspasemediated cleavage of cytoskeletal proteins, a hallmark of apoptosis (Figure 2G; Table S13). Thinning of the fibrous cap is also attributed to release of MMPs that degrade the ECM by vSMCs or vSMC-derived macrophages.⁴⁵ Additionally, *Trem2*+ foamy macrophage DEGs were enriched for ECM proteoglycans, integrin cell surface interactions, ECM organization, and autophagy (Figure S5A; Table S13). DEGs from the remaining macrophage subtypes were enriched for immune and inflammatory pathways, including mitophagy, antigen processing cross presentation, and interferon and cytokine signaling in inflammatory macrophages (Figure S5B; Table S13); C type lectin receptors, death receptor signaling, and interleukin and cytokine signaling in monocytes (Figure S5C; Table S12); interferon signaling, TGFβ signaling, and antigen processing and presentation in resident macrophages (Figure S5D; Table S13).

Previously, TMAO has also been shown to directly act on platelets to promote platelet hyperresponsiveness and a prothrombotic phenotype by altering calcium release from intracellular stores. 46 Although platelets could not be captured in our aorta scRNAseq, we observed a potential downstream effect of platelet response to TMAO as endothelial cell DEGs in our data were significantly enriched for response to elevated platelet cytosolic calcium and platelet activation signaling and aggregation (Figure S6).

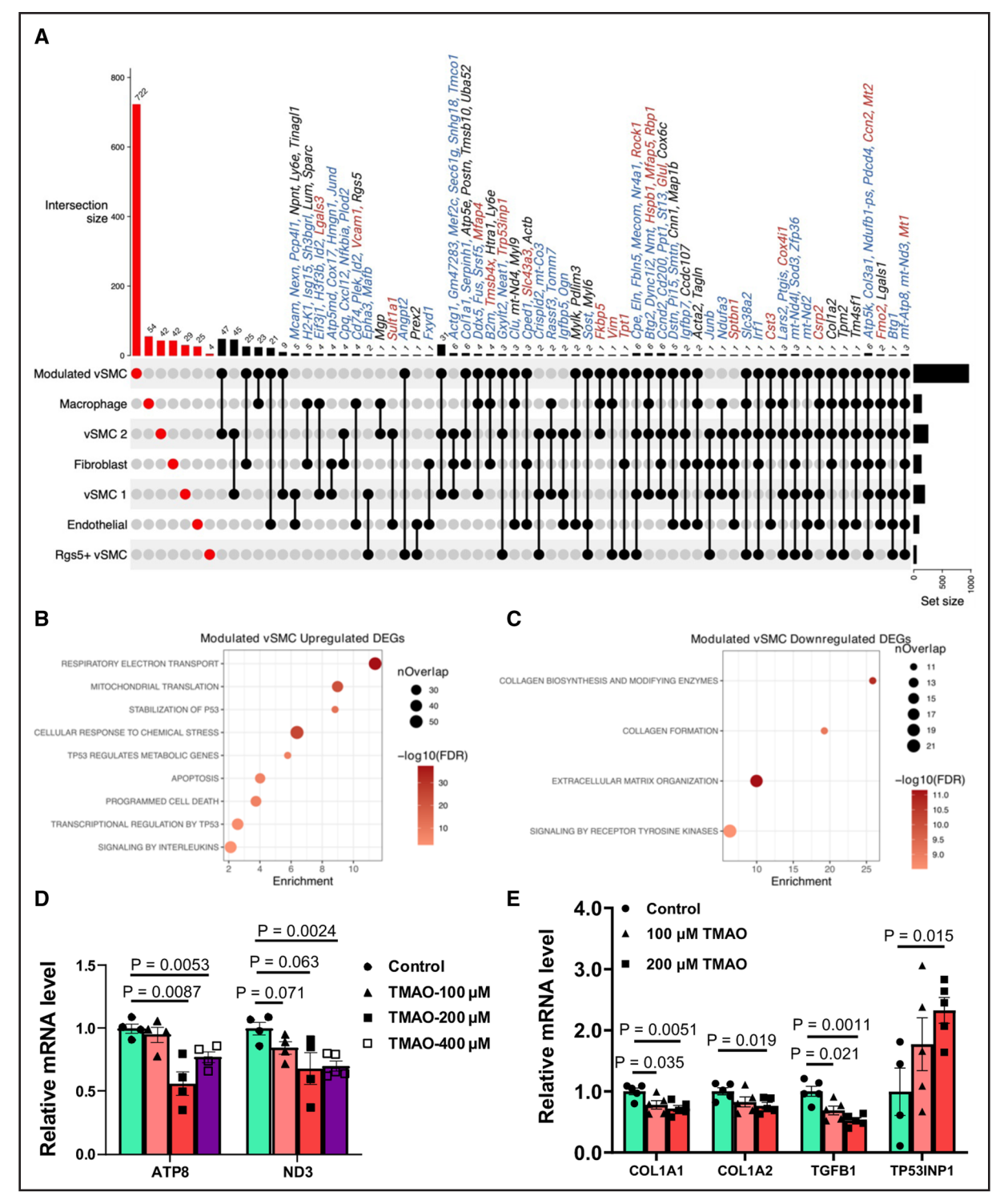


Figure 3. Shared and cell type-specific differentially expressed genes (DEGs) induced by trimethylamine-N-oxide (TMAO) in major aortic cell types.

A, Shared and cell type–specific DEGs (false discovery rate [FDR] <0.05) induced by TMAO feeding in major aortic cell types recovered in single-cell RNA-sequencing. DEGs unique to a cell type are highlighted in red in the upset plot and histogram, and shared DEGs are indicated in black. The histogram above each plot indicates the DEG counts for each category. DEG direction is indicated by the color of the gene name: red: upregulated in high-cholesterol (HC)+TMAO vs HC, blue: downregulated in HC+TMAO vs HC, black: cell type–dependent. **B** and **C**, Top representative pathways from Reactome enriched for upregulated and downregulated modulated vascular smooth muscle cell (vSMC) DEGs (FDR<0.05), respectively. **D**, *ATP8* and *ND3* expression in immortalized human aortic smooth muscle cells with TMAO stimulus. **E**, *COL1A1*, *COL1A2*, *TGFB1*, and *TP53INP1* gene expression in primary human coronary artery smooth muscle cells with TMAO stimulus. One-way ANOVA with Tukey post hoc test was used to determine statistical significance.

Within-Cell-Type Regulators of TMAO DEGs and Pathways in vSMCs

To complement the DEG and pathway analysis and elucidate intracellular regulatory cascades induced by TMAO feeding, we constructed cell type-specific directed GRNs using an unbiased gradient boosting method SCING.³⁹ We identified subnetworks (termed modules) associated with TMAO in each cell type. For modulated vSMCs, modules significantly associated with TMAO

confirmed the ECM and apoptosis pathways revealed above through M11 (ECM organization and biological adhesion) and M19 (regulation of cell death; Figure 4A). We also identified M4 (translation initiation and protein transport) and M1 and M2 (electron transport chain and mitochondrion organization; Figure 4A). We further retrieved the top interconnected genes within each module as potential regulators, as they signify centrality and importance within the network structure.⁴⁷ For example, *Tnn*, *Col11a2*, and *Col9a3* were potential regulators of

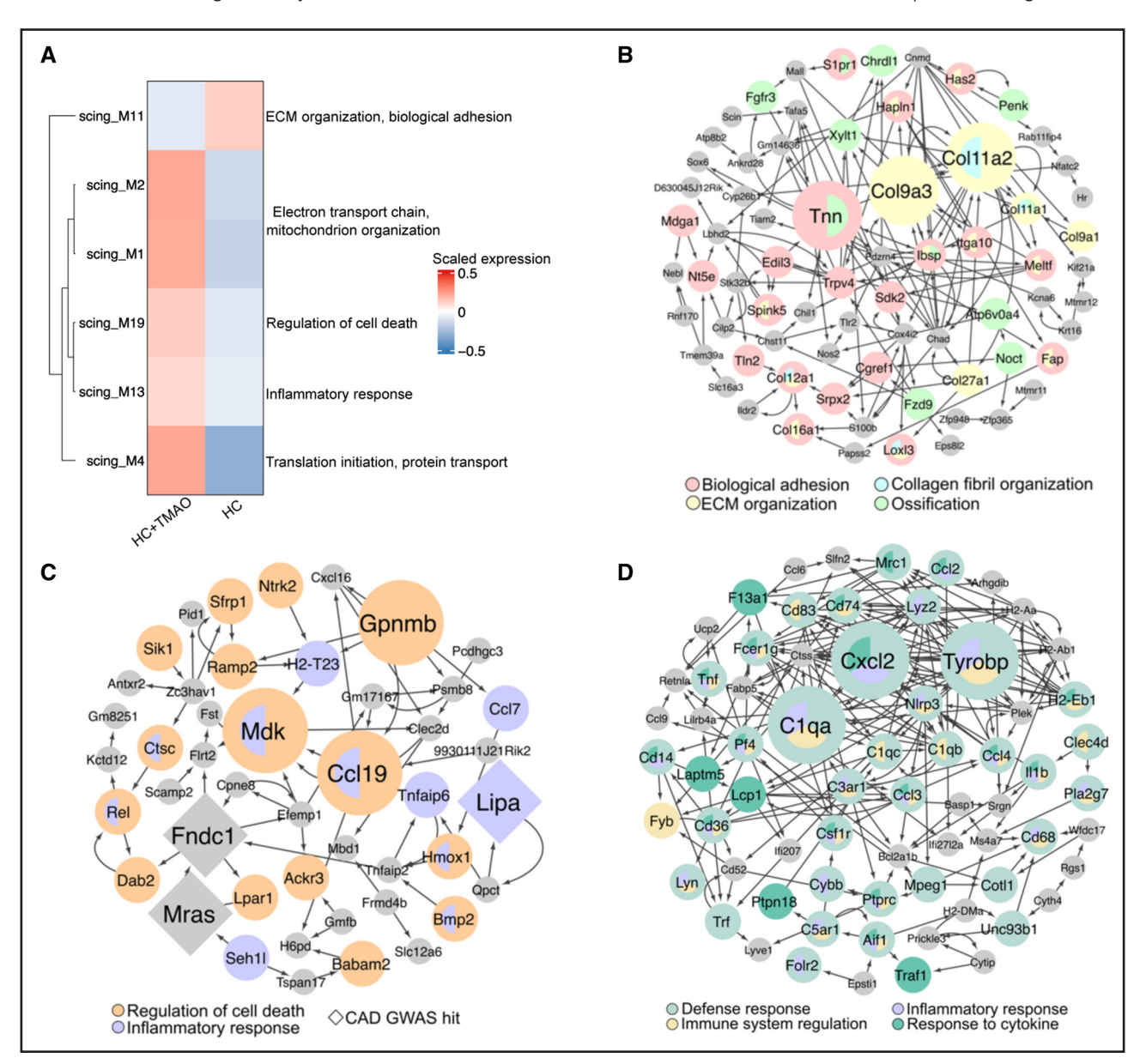


Figure 4. Modulated vascular smooth muscle cell (vSMC) gene regulatory networks significantly associated with trimethylamine-N-oxide (TMAO) in the diet.

A, Top modulated vSMC gene regulatory network (GRN) modules significantly associated with TMAO feeding by SCING. The top biological pathways enriched for the genes in each network are listed. Statistical significance of TMAO association for each module was determined by Wilcoxon rank-sum test. *P* values were adjusted by Bonferroni. Adjusted *P*<0.0001 for all network modules shown. **B** through **D**, Network structures of directed SCING modules M11, M19, and M13, respectively. The direction of the interaction is denoted by arrows in the networks. The top 3 most interconnected nodes involved in the relevant pathways for each network and known human coronary artery disease genome-wide association study (GWAS) hits are highlighted by larger size. GWAS hits are also denoted by the diamond shape. Genes in the pathways enriched in each module are annotated by different colors. CAD indicates coronary artery disease; ECM, extracellular matrix; and HC, high-cholesterol.

module M11, enriched for ECM organization and biological adhesion (Figure 4B). *Gpnmb*, *Mdk*, and *Ccl19* were regulators of the cell death module M19 (Figure 4C). Also, this cell death regulation GRN included 3 known human coronary artery disease genome-wide association study hits: *Fndc1*, *Mras*, and *Lipa*. For the inflammation module M13, we identified *Tyrobp*, *C1qa*, and *Cxcl2* as potential regulators (Figure 4D).

TMAO Impacts Cell-Cell Communication and External Signaling Regulators Targeting Modulated vSMCs and Macrophage Subtypes

To further understand the atherosclerotic microenvironment impacted by TMAO, we predicted cell-cell communications involving the major cell types within the lesion. Ligand-receptor-based CellChat analysis indicated that TMAO increased modulated vSMC-endothelial and endothelial-endothelial interactions and enhanced outgoing signals from Trem2+ macrophage and vSMCderived macrophage (Figure 5A and 5B). TMAO also increased interactions from vSMC-derived macrophages to modulated vSMCs (Figure 5A). For modulated vSMCs, collagen, NCAM, and laminin signaling, which are all related to ECM organization, were predicted to decrease as both incoming and outgoing interactions, whereas SPP1 signaling was predicted to increase as an incoming and outgoing signal (Figure 5C). Spp1 was significantly upregulated in modulated vSMCs with TMAO feeding in our scRNAseg and is a well-known biomarker elevated in atherosclerotic patients that can track plaque severity and cardiovascular event mortality^{48,49} (Figure S7A).

We next identified external signaling regulators of modulated vSMC DEGs involved in the upregulation of apoptosis and downregulation of ECM organization using NicheNet. Apoptosis-related DEGs in modulated vSMCs were predicted to be regulated by ligands from multiple cell types, such as Tgfb1, Ptgs2, Agrn, Efna, Adam17, and Trf, and by inflammatory macrophage ligand Hbegf, monocyte Thbs1, and endothelial ligand Edn1 (Figure 5D). ECM-related DEGs in modulated vSMCs were predicted to be regulated by Trem2+ macrophage ligand Spp1, inflammatory macrophage ligand Plau, endothelial ligands Edn1 and Bmp6, and various ligands shared across cell types, including Tgfb1, II1b, Timp1, and Mmp9 (Figure 5D). Tgfb1, one of the master regulators of ECM molecule secretion, was predicted to be a shared ligand between monocytes and inflammatory macrophages to regulate ECM genes in modulated vSMCs. We confirmed the direct effect of TMAO on significantly downregulating Tgfb1 in RAW cells (Figure S7B). We further predicted ligands that target DEGs of macrophage subtypes, revealing potential regulatory ligands from endothelial cells (Edn1, Bmp6) and from other macrophage subtypes (Bmp2, Spp1; Figure 5E).

TMAO Reduces the Fibrous Cap Size in Atherosclerotic Lesions

As we have identified apoptosis and ECM organization as key upregulated and downregulated processes, respectively, in modulated vSMCs with TMAO feeding, we hypothesized that TMAO feeding would reduce the fibrous cap to promote plaque instability. We therefore examined the fibrous caps of Ldlr-/- female mice fed HC+TMAO or HC diets for 5 months. Thinner fibrous caps overlaying the atherosclerotic lesion imply plaque vulnerability and increased likelihood of rupture, so we used TagIn immunostaining to identify and measure cap thickness. We utilized depth of TagIn+ cells from the lumen, representing the fibrous cap, as a marker of plaque stability in aortic root lesions. Mice fed the HC+TMAO diet exhibited significantly decreased fibrous cap thickness compared with mice fed the HC diet (Figure 6A and 6C). There was no significant difference in CD68+ macrophage percentage in the lesion between HC+TMAO and HC groups (Figure 6A and 6D). We further observed that TMAO feeding significantly decreased the percentage of collagen deposition in lesions (Figure 6B and 6E).

DISCUSSION

This study investigates TMAO in the context of cellular heterogeneity of the lesion microenvironment and characterizes the effect of TMAO on the gene expression signatures of in vivo disease-specific vascular cell types. Our studies highlight the particular importance of modulated vSMCs and vSMC-derived macrophages, 2 key atherosclerosis-associated cell types, in TMAO actions. Our findings from differential gene expression analysis, intracellular GRN modeling, and cell-cell communication predictions converged to reveal that TMAO upregulates apoptotic gene signatures and downregulates ECM organization and collagen formation gene signatures in atheroprotective modulated vSMCs. The direct effect of TMAO on these cell types and pathways was confirmed via in vitro exposure studies in vSMC and macrophage cell lines. As key pathways known to contribute to plaque instability include decreased collagen production at the fibrous cap by phenotypically switched vSMCs and increased collagen degradation via macrophage-released MMPs, our scRNAseq results suggest TMAO may promote plaque instability and likelihood of rupture, which is supported by the thinner fibrous caps and decreased collagen deposition with TMAO.

In addition to standard DEG and pathway analysis, which highlighted cell type-specific alterations such as downregulation of ECM genes and an increase in apoptosis in modulated vSMCs, our network analyses offered comprehensive insights into the regulatory cascades within and across cell types via various regulators. This included decreased collagen and laminin signaling in

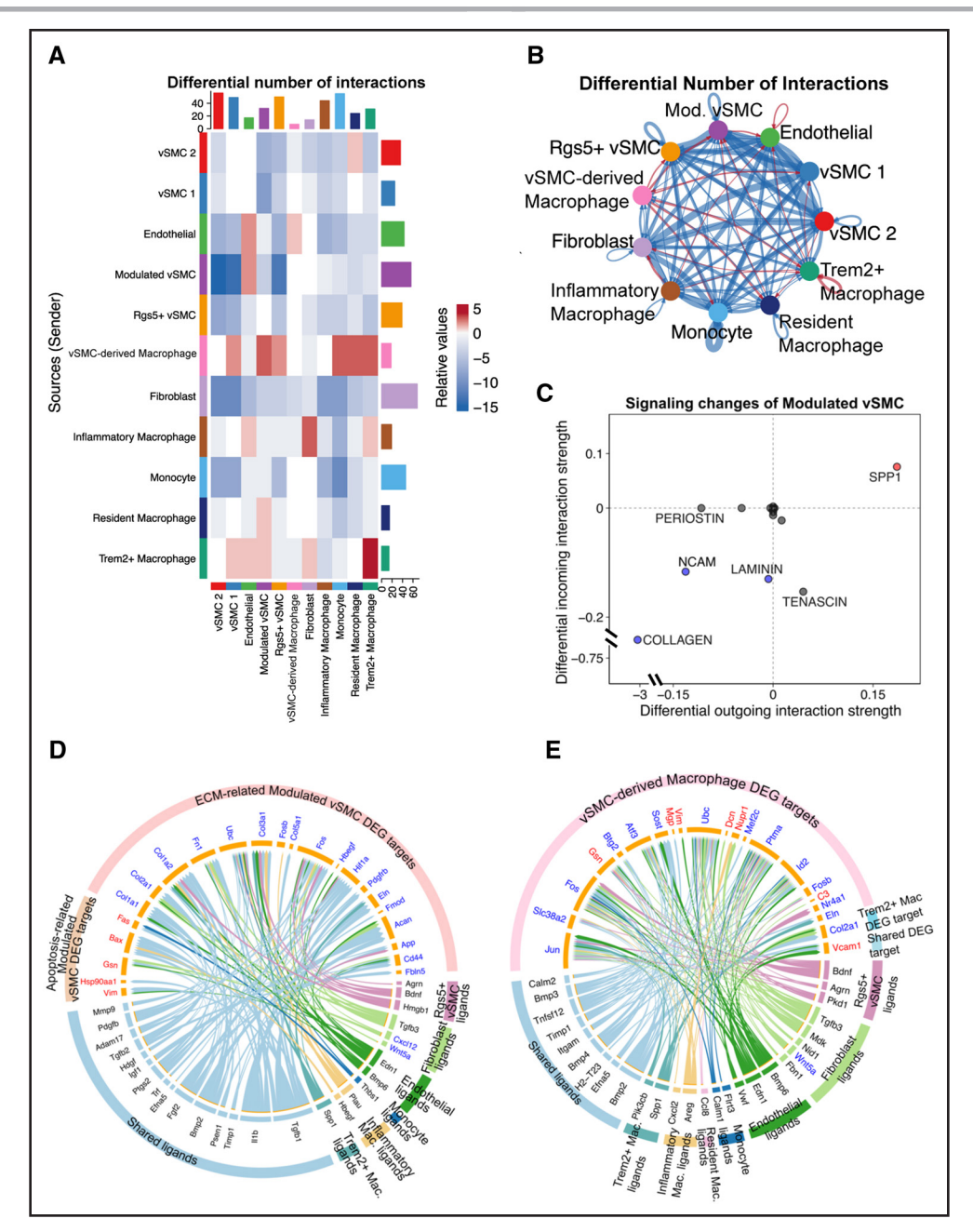


Figure 5. Trimethylamine-N-oxide (TMAO) alters cell-cell communications between major cell types involved in atherosclerosis progression.

A, Predicted differential number of interactions between sender (rows) and receiver (columns) cell types comparing high-cholesterol (HC)+TMAO and HC by CellChat. In the heatmap, red represents increased signaling with TMAO feeding, and blue represents decreased signaling. B, Predicted differential number of interactions in the cell-cell communication network between HC+TMAO and HC by CellChat. The color of the network edges represents increased (red) or decreased (blue) signaling with TMAO feeding. C, Specific incoming and outgoing signaling pathways predicted to change in modulated vascular smooth muscle cells (vSMCs) between HC+TMAO and HC by CellChat. Signaling pathways increased and decreased as both incoming and outgoing signals are highlighted in red and blue, respectively. D, Top ligands predicted by NicheNet to target the modulated vSMC differentially expressed gene (DEGs) involved in apoptosis or ECM (extracellular matrix) organization. E, Top ligands predicted by NicheNet to target the vSMC-derived macrophage and Trem2+ macrophage DEGs. In D and E, DEG direction is indicated by red (upregulated with TMAO) or blue (downregulated with TMAO). Mac indicates macrophage; and Mod, vSMC, modulated vSMC.

modulated vSMCs, increased *Spp1* signaling in modulated vSMCs, and predicted *Spp1* signaling from *Trem2*⁺ macrophages targeting modulated vSMC ECM-related DEGs. Interestingly, the cell type-specific GRNs also

highlighted human coronary artery disease genome-wide association study hits *LIPA*, *MRAS*, and *FNDC1*⁵⁰⁻⁵² in a modulated vSMC subnetwork enriched for regulation of cell death and inflammatory response.⁵⁰ This mechanistic

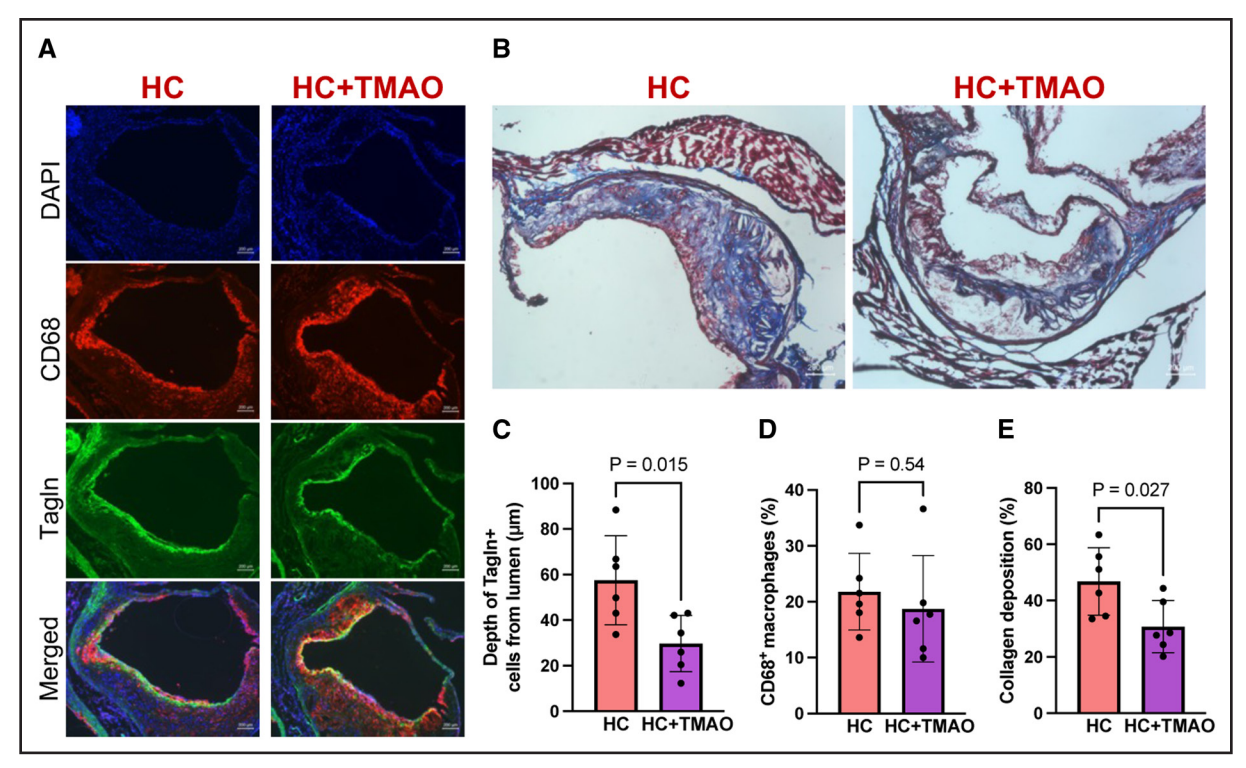


Figure 6. Trimethylamine-N-oxide (TMAO) decreases the lesional fibrous cap and collagen deposition. A, Representative immunofluorescence staining of aortic root lesions and the fibrous cap using Tagln (transgelin) and CD68 (cluster of differentiation 68) in high-cholesterol (HC)+TMAO and HC groups. **B**, Representative Masson's trichrome staining of aortic root lesions in HC+TMAO and HC groups. **C**, Depth of Tagln+ cells from lumen (μm) measurements for HC+TMAO and HC groups (15 evenly spaced measurements/mouse). **D**, Percentage of CD68+ macrophages in aortic root lesions in HC+TMAO and HC groups. **E**, Area of collagen deposition in aortic root lesions in HC+TMAO and HC groups. Statistical significance was determined with unpaired *t* test. DAPI indicates 4′,6-diamidino-2-phenylindole.

interpretation of the genome-wide association study variants further highlights their cellular context and connection to TMAO risk. One method for cell-cell communication prediction, CellChat, supported vSMC-derived macrophage and modulated vSMC communication, whereas the second method used, Nichenet, did not. The stringent threshold used in Nichenet filtered out potential ligands from vSMC-derived macrophages that target ECM- and apoptosis-related modulated vSMC DEGs. Because these 2 methods investigate complementary aspects of cell-cell communication, we consider the CellChat results to provide evidence for cell-cell communication between vSMC-derived macrophages and modulated vSMCs.

It is important to note that we identified various ECM and collagen genes as significantly downregulated in modulated vSMCs by TMAO. However, a previous study found no significant impact of TMAO on plaque burden or histological features, including collagen, when feeding *Ldlr*— or *ApoE*— mice a high- versus low-choline high-fat, HC diet. This difference in findings may be attributed to differences in diets, mouse age, and the experimental measure used to characterize plaque instability (ie, scRNAseq gene expression versus histology). However, our findings align with other previous work. 346

Our study shows that TMAO promotes apoptosis in the context of atherosclerosis and to identify a subset of atheroprotective modulated vSMCs to be most susceptible to TMAO. This agrees with a recent study revealing a TMAO to abdominal aortic aneurysm link via upregulation of endoplasmic reticulum stress and apoptosis genes in aortic vSMCs.³

Although our findings elucidated the impact of TMAO across vascular cell types, we also acknowledge the limitations of our study. First, our study focuses on gene expression signatures via scRNAseq and in vitro gene expression validation. Additional validation at protein and functional levels is warranted. Second, certain cell types recovered were low in population number, such as T cells and B cells, thereby limiting the power to perform differential gene expression analysis. Third, here we focused on measuring the thickness of the fibrous cap, collagen deposition, and macrophage content, but additional plaque instability measures such as platelet activation and intraplaque hemorrhage, could be examined. Fourth, we acknowledge that our control NL mouse group was not age-matched with the HC and HC+TMAO groups, but our results when comparing HC versus NL recapitulated previously known findings. 20,53 Further, our primary focus was not HC versus NL comparison but on

the effect of TMAO, where age was matched between the HC+TMAO and HC groups. Lastly, we focused on female mice due to larger atherosclerotic lesion sizes in this sex, and future studies of males are warranted.

In summary, our findings provide molecular and phenotypic evidence that TMAO may contribute to plaque instability through regulating ECM degradation and apoptosis in cell subtypes that arise with atherosclerosis progression, such as modulated vSMCs and vSMC-derived macrophages.

ARTICLE INFORMATION

Received May 19, 2025; accepted July 22, 2025.

Affiliations

Department of Integrative Biology and Physiology (J.C., M.C., I.C., G.Z., I.S.A., G.D., X.Y.), and Department of Human Genetics (H.A., A.J.L.), Molecular, Cellular, and Integrative Physiology Interdepartmental Program (J.C.), Division of Cardiology, Department of Medicine CA (J.C., S.S., S.G., M.T.H., Z.Z., R.C., Y.-c.W., B.J.B., H.A., A.J.L., D.M.S.), Bioinformatics Interdepartmental Program (M.C.), Molecular Toxicology Interdepartmental Program (I.C.), Department of Microbiology, Immunology and Molecular Genetics (H.A., A.J.L.), Department of Anesthesiology and Perioperative Medicine, David Geffen School of Medicine (H.C.), Institute for Quantitative and Computational Biosciences (X.Y.), and Molecular Biology Institute (X.Y.), University of California, Los Angeles. Department of Cardiovascular Medicine, Heart, Vascular, and Thoracic Institute (Z.W., S.L.H.) and Department of Cardiovascular and Metabolic Sciences, Lerner Research Institute (Z.W., S.L.H.), Cleveland Clinic, Ohio.

Acknowledgments

The authors thank the University of California, Los Angeles Technology Center for Genomics and Bioinformatics for the sequencing of our single-cell data; Dr Juyong B. Kim for sharing his expertise in single-cell protocols; Dr Clint L. Miller for kindly providing the immortalized human coronary artery vascular smooth muscle cells; and the laboratories of Drs Thomas Vallim, Elizabeth Tarling, and Peter Tontonoz for use of their microscopy facilities.

Sources of Funding

The study was supported by National Institutes of Health/National Heart, Lung, and Blood Institute R01 HL148110 (D.M. Shih, H. Allayee, and X. Yang) and the Asrican Sophie and Jack Award (J. Cheng).

Disclosures

None

Supplemental Material

Tables S1-S13 Figure S1-S7 Major Resources Table

REFERENCES

- Fung TC, Olson CA, Hsiao EY. Interactions between the microbiota, immune and nervous systems in health and disease. *Nat Neurosci.* 2017;20:145– 155. doi: 10.1038/nn.4476
- Wang Z, Klipfell E, Bennett BJ, Koeth R, Levison BS, Dugar B, Feldstein AE, Britt EB, Fu X, Chung YM, et al. Gut flora metabolism of phosphatidylcholine promotes cardiovascular disease. *Nature*. 2011;472:57–63. doi: 10.1038/nature09922
- Benson TW, Conrad KA, Li XS, Wang Z, Helsley RN, Schugar RC, Coughlin TM, Wadding-Lee C, Fleifil S, Russell HM, et al. Gut microbiota-derived trimethylamine N-oxide contributes to abdominal aortic aneurysm through inflammatory and apoptotic mechanisms. Circulation. 2023;147:1079–1096. doi: 10.1161/CIRCULATIONAHA.122.060573
- Wilson Tang WH, Wang Z, Levison BS, Koeth RA, Britt EB, Fu X, Wu Y, Hazen SL. Intestinal microbial metabolism of phosphatidylcholine and cardiovascular risk. N Engl J Med. 2013;368:1575–1584. doi: 10.1056/NEJMoa1109400

- Zhu W, Buffa JA, Wang Z, Warrier M, Schugar R, Shih DM, Gupta N, Gregory JC, Org E, Fu X, et al. Flavin monooxygenase 3, the host hepatic enzyme in the metaorganismal trimethylamine N-oxide-generating pathway, modulates platelet responsiveness and thrombosis risk. J Thromb Haemost. 2018;16:1857–1872. doi: 10.1111/jth.14234
- Tang WHW, Wang Z, Fan Y, Levison B, Hazen JE, Donahue LM, Wu Y, Hazen SL. Prognostic value of elevated levels of intestinal microbegenerated metabolite trimethylamine-N-oxide in patients with heart failure. *J Am Coll Cardiol*. 2014;64:1908–1914. doi: 10.1016/j.jacc.2014.02.617
- Tang WHW, Wang Z, Shrestha K, Borowski AG, Wu Y, Troughton RW, Klein AL, Hazen SL. Intestinal microbiota-dependent phosphatidylcholine metabolites, diastolic dysfunction, and adverse clinical outcomes in chronic systolic heart failure. J Card Fail. 2015;21:91–96. doi: 10.1016/j.cardfail.2014.11.006
- Bennett BJ, de Aguiar Vallim TO, Wang Z, Shih DM, Meng Y, Gregory J, Allayee H, Lee R, Graham M, Crooke R, et al. Trimethylamine-N-oxide, a metabolite associated with atherosclerosis, exhibits complex genetic and dietary regulation. *Cell Metab.* 2013;17:49–60. doi: 10.1016/j.cmet.2012.12.011
- Senthong V, Li XS, Hudec T, Coughlin J, Wu Y, Levison B, Wang Z, Hazen SL, Tang WHW. Plasma trimethylamine N-oxide, a gut microbe-generated phosphatidylcholine metabolite, is associated with atherosclerotic Burden. J Am Coll Cardiol. 2016;67:2620–2628. doi: 10.1016/j.jacc.2016.03.546
- Koeth RA, Wang Z, Levison BS, Buffa JA, Org E, Sheehy BT, Britt EB, Fu X, Wu Y, Li L, et al. Intestinal microbiota metabolism of L-carnitine, a nutrient in red meat, promotes atherosclerosis. *Nat Med.* 2013;19:576–585. doi: 10.1038/nm.3145
- Warrier M, Shih DM, Burrows AC, Ferguson D, Gromovsky AD, Brown AL, Marshall S, McDaniel A, Schugar RC, Wang Z, et al. The TMAO-generating enzyme flavin monooxygenase 3 is a central regulator of cholesterol balance. *Cell Rep.* 2015;10:326–338. doi: 10.1016/j.celrep.2014.12.036
- Shih DM, Wang Z, Lee R, Meng Y, Che N, Charugundla S, Qi H, Wu J, Pan C, Brown JM, et al. Flavin containing monooxygenase 3 exerts broad effects on glucose and lipid metabolism and atherosclerosis. *J Lipid Res.* 2015;56:22–37. doi: 10.1194/jlr.M051680
- Seldin MM, Meng Y, Qi H, Zhu W, Wang Z, Hazen SL, Lusis AJ, Shih DM. Trimethylamine N-oxide promotes vascular inflammation through signaling of Mitogen-Activated protein kinase and nuclear factor-κB. J Am Heart Assoc. 2767;5:e00. doi: 10.1161/jaha.115.002767
- Chen M, Zhu X, Ran L, Lang H, Yi L, Mi M. Trimethylamine-N-oxide induces vascular inflammation by activating the NLRP3 inflammasome through the SIRT3-SOD2-mtROS signaling pathway. J Am Heart Assoc. 2017;6:e006347. doi: 10.1161/JAHA.117.006347
- Saaoud F, Liu L, Xu K, Cueto R, Shao Y, Lu Y, Sun Y, Snyder NW, Wu S, Yang L, et al. Aorta- and liver-generated TMAO enhances trained immunity for increased inflammation via ER stress/mitochondrial ROS/glycolysis pathways. *JCl Insight*. 2023;8:e158183. doi: 10.1172/jci.insight.158183
- Liu H, Jia K, Ren Z, Sun J, Pan LL. PRMT5 critically mediates TMAOinduced inflammatory response in vascular smooth muscle cells. *Cell Death Dis.* 2022;13:1–11. doi: 10.1038/s41419-022-04719-7
- 17. Tan Y, Sheng Z, Zhou P, Liu C, Zhao H, Song L, Li J, Zhou J, Chen Y, Wang L, et al. Plasma trimethylamine N-Oxide as a novel biomarker for plaque rupture in patients with ST-Segment-elevation myocardial infarction. *Circ Cardiovasc Interv.* 2019;12:e007281. doi: 10.1161/CIRCINTERVENTIONS.118.007281
- Koay YC, Chen YC, Wali JA, Luk AWS, Li M, Doma H, Reimark R, Zaldivia MTK, Habtom HT, Franks AE, et al. Plasma levels of trimethylamine-N-oxide can be increased with "healthy" and 'unhealthy' diets and do not correlate with the extent of atherosclerosis but with plaque instability. Cardiovasc Res. 2021;117:435–449. doi: 10.1093/cvr/cvaa094
- Shi W, Huang Y, Yang Z, Zhu L, Yu B. Reduction of TMAO level enhances the stability of carotid atherosclerotic plaque through promoting macrophage M2 polarization and efferocytosis. *Biosci Rep.* 2021;41:BSR20204250. doi: 10.1042/BSR20204250
- Wirka RC, Wagh D, Paik DT, Pjanic M, Nguyen T, Miller CL, Kundu R, Nagao M, Coller J, Koyano TK, et al. Atheroprotective roles of smooth muscle cell phenotypic modulation and the TCF21 disease gene as revealed by single-cell analysis. *Nat Med.* 2019;25:1280–1289. doi: 10.1038/s41591-019-0512-5
- Daugherty A, Rateri DL. Development of experimental designs for atherosclerosis studies in mice. *Methods*. 2005;36:129–138. doi: 10.1016/j.ymeth.2004.11.008
- Paigen B, Holmes PA, Mitchell D, Albee D. Comparison of atherosclerotic lesions and HDL-lipid levels in male, female, and testosterone-treated female mice from strains C57BL/6, BALB/c, and C3H. Atherosclerosis. 1987;64:215–221. doi: 10.1016/0021-9150(87)90249-8

- Pan H, Xue C, Auerbach BJ, Fan J, Bashore AC, Cui J, Yang DY, Trignano SB, Liu W, Shi J, et al. Single-Cell genomics reveals a novel cell state during smooth muscle cell phenotypic switching and potential therapeutic targets for atherosclerosis in mouse and human. *Circulation*. 2020;142:2060– 2075. doi: 10.1161/CIRCULATIONAHA.120.048378
- Kim K, Shim D, Lee JS, Zaitsev K, Williams JW, Kim KW, Jang MY, Seok Jang H, Yun TJ, Lee SH, et al. Transcriptome analysis reveals nonfoamy rather than foamy plaque macrophages are proinflammatory in atherosclerotic murine models. *Circ Res.* 2018;123:1127–1142. doi: 10.1161/CIRCRESAHA.118.312804
- Angueira AR, Sakers AP, Holman CD, Cheng L, Arbocco MN, Shamsi F, Lynes MD, Shrestha R, Okada C, Batmanov K, et al. Defining the lineage of thermogenic perivascular adipose tissue. *Nat Metab.* 2021;3:469–484. doi: 10.1038/s42255-021-00380-0
- Fleming SJ, Chaffin MD, Arduini A, Akkad AD, Banks E, Marioni JC, Philippakis AA, Ellinor PT, Babadi M. Unsupervised removal of systematic background noise from droplet-based single-cell experiments using CellBender. Nat Methods. 2023;20:1323–1335. doi: 10.1038/s41592-023-01943-7
- Satija R, Farrell JA, Gennert D, Schier AF, Regev A. Spatial reconstruction of single-cell gene expression data. *Nat Biotechnol.* 2015;33:495–502. doi: 10.1038/nbt.3192
- Butler A, Hoffman P, Smibert P, Papalexi E, Satija R. Integrating single-cell transcriptomic data across different conditions, technologies, and species. Nat Biotechnol. 2018;36:411–420. doi: 10.1038/nbt.4096
- Cochain C, Vafadarnejad E, Arampatzi P, Pelisek J, Winkels H, Ley K, Wolf D, Saliba AE, Zernecke A. Single-Cell RNA-Seq Reveals the transcriptional landscape and heterogeneity of aortic macrophages in murine atherosclerosis. Circ Res. 2018;122:1661–1674. doi: 10.1161/CIRCRESAHA.117.312509
- Kan H, Zhang K, Mao A, Geng L, Gao M, Feng L, You Q, Ma X. Single-cell transcriptome analysis reveals cellular heterogeneity in the ascending aortas of normal and high-fat diet-fed mice. *Exp Mol Med.* 2021;53:1379–1389. doi: 10.1038/s12276-021-00671-2
- Phipson B, Sim CB, Porrello ER, Hewitt AW, Powell J, Oshlack A. propeller: testing for differences in cell type proportions in single cell data. *Bioinformatics*. 2022;38:4720–4726. doi: 10.1093/bioinformatics/btac582
- Street K, Risso D, Fletcher RB, Das D, Ngai J, Yosef N, Purdom E, Dudoit S. Slingshot: cell lineage and pseudotime inference for single-cell transcriptomics. *BMC Genomics*. 2018;19:477. doi: 10.1186/s12864-018-4772-0
- Joshi-Tope G, Gillespie M, Vastrik I, D'Eustachio P, Schmidt E, de Bono B, Jassal B, Gopinath GR, Wu GR, Matthews L, et al. Reactome: a knowledgebase of biological pathways. *Nucleic Acids Res.* 2005;33:D428–D432. doi: 10.1093/nar/gki072
- Gillespie M, Jassal B, Stephan R, Milacic M, Rothfels K, Senff-Ribeiro A, Griss J, Sevilla C, Matthews L, Gong C, et al. The reactome pathway knowledgebase 2022. Nucleic Acids Res. 2022;50:D687-D692. doi: 10.1093/nar/gkab1028
- O'Leary K, Zheng D. Metacell-based differential expression analysis identifies cell type specific temporal gene response programs in COVID-19 patient PBMCs. npj Syst Biol Appl. 2024;10:1–13. doi: 10.1038/s41540-024-00364-2
- Baran Y, Bercovich A, Sebe-Pedros A, Lubling Y, Giladi A, Chomsky E, Meir Z, Hoichman M, Lifshitz A, Tanay A. MetaCell: analysis of single-cell RNA-seq data using K-nn graph partitions. *Genome Biol.* 2019;20:206. doi: 10.1186/s13059-019-1812-2
- Morabito S, Reese F, Rahimzadeh N, Miyoshi E, Swarup V. hdWGCNA identifies co-expression networks in high-dimensional transcriptomics data. *Cell Rep Methods*. 2023;3:100498. doi: 10.1016/j.crmeth.2023.100498

- Love MI, Huber W, Anders S. Moderated estimation of fold change and dispersion for RNA-seq data with DESeq2. Genome Biol. 2014;15:550. doi: 10.1186/s13059-014-0550-8
- Littman R, Cheng M, Wang N, Peng C, Yang X. SCING: Inference of robust, interpretable gene regulatory networks from single cell and spatial transcriptomics. iScience. 2023;26:107124. doi: 10.1016/j.isci.2023.107124
- Shannon P, Markiel A, Ozier O, Baliga NS, Wang JT, Ramage D, Amin N, Schwikowski B, Ideker T. Cytoscape: a software environment for integrated models of biomolecular interaction networks. *Genome Res.* 2003;13:2498– 2504. doi: 10.1101/qr.1239303
- Jin S, Guerrero-Juarez CF, Zhang L, Chang I, Ramos R, Kuan CH, Myung P, Plikus MV, Nie O. Inference and analysis of cell-cell communication using Cell-Chat. Nat Commun. 2021;12:1088. doi: 10.1038/s41467-021-21246-9
- Browaeys R, Saelens W, Saeys Y. NicheNet: modeling intercellular communication by linking ligands to target genes. *Nat Methods*. 2020;17:159–162. doi: 10.1038/s41592-019-0667-5
- Newman AAC, Serbulea V, Baylis RA, Shankman LS, Bradley X, Alencar GF, Owsiany K, Deaton RA, Karnewar S, Shamsuzzaman S, et al. Multiple cell types contribute to the atherosclerotic lesion fibrous cap by PDGFRβ and bioenergetic mechanisms. *Nat Metab.* 2021;3:166–181. doi: 10.1038/s42255-020-00338-8
- 44. von der Thüsen JH, van Vlijmen BJM, Hoeben RC, Kockx MM, Havekes LM, van Berkel TJC, Biessen EAL. Induction of atherosclerotic plaque rupture in apolipoprotein E^{-/-} mice after adenovirus-mediated transfer of p53. Circulation. 2002;105:2064–2070. doi: 10.1161/01.cir.0000015502.97828.93
- Basatemur GL, Jørgensen HF, Clarke MCH, Bennett MR, Mallat Z. Vascular smooth muscle cells in atherosclerosis. Nat Rev Cardiol. 2019;16:727–744. doi: 10.1038/s41569-019-0227-9
- Zhu W, Gregory JC, Org E, Buffa JA, Gupta N, Wang Z, Li L, Fu X, Wu Y, Mehrabian M, et al. Gut microbial metabolite TMAO enhances platelet hyperreactivity and thrombosis risk. *Cell.* 2016;165:111-124. doi: 10.1016/j.cell.2016.02.011
- Cheng J, Cheng M, Lusis AJ, Yang X. Gene regulatory networks in coronary artery disease. *Curr Atheroscler Rep.* 2023;25:1013–1023. doi: 10.1007/s11883-023-01170-7
- Ohmori R, Momiyama Y, Taniguchi H, Takahashi R, Kusuhara M, Nakamura H, Ohsuzu F. Plasma osteopontin levels are associated with the presence and extent of coronary artery disease. *Atherosclerosis*. 2003;170:333–337. doi: 10.1016/s0021-9150(03)00298-3
- Momiyama Y, Ohmori R, Fayad ZA, Kihara T, Tanaka N, Kato R, Taniguchi H, Nagata M, Nakamura H, Ohsuzu F. Associations between plasma osteopontin levels and the severities of coronary and aortic atherosclerosis. *Athero*sclerosis. 2010;210:668–670. doi: 10.1016/j.atherosclerosis.2009.12.024
- Wild PS, Zeller T, Schillert A, Szymczak S, Sinning CR, Deiseroth A, Schnabel RB, Lubos E, Keller T, Eleftheriadis MS, et al. A genome-wide association study identifies LIPA as a susceptibility gene for coronary artery disease. Circ Cardiovasc Genet. 2011;4:403-412. doi: 10.1161/CIRCGENETICS.110.958728
- Liu L, You L, Tan L, Wang DW, Cui W. Genetic insight into the role of MRAS in coronary artery disease risk. Gene. 2015;564:63-66. doi: 10.1016/j.gene.2015.03.041
- 52. Lin K, Zhang L, Wang Y, Li J, Xu Y, Che D, Mai H, Yu H, Fu L, Wei B, et al. FNDC1 Polymorphism (rs3003174 C > T) Increased the incidence of coronary artery aneurysm in patients with Kawasaki disease in a southern Chinese population. *J Inflamm Res.* 2021;14:2633-2640. doi: 10.2147/JIR.S311956
- Zhang F, Guo X, Xia Y, Mao L. An update on the phenotypic switching of vascular smooth muscle cells in the pathogenesis of atherosclerosis. *Cell Mol Life Sci.* 2021;79:6. doi: 10.1007/s00018-021-04079-z